Published in final edited form as:
Biochemistry. 2012 September 11; 51(36): 7128–7137. doi:10.1021/bi300920m.

Metal Ion Involvement in the Allosteric Mechanism of *Escherichia coli* Aspartate Transcarbamoylase

Gregory M. Cockrell and **Evan R. Kantrowitz***
Boston College, Department of Chemistry, Merkert Chemistry Center, Chestnut Hill, MA 02467

Abstract

E. coli aspartate transcarbamoylase (ATCase) allosterically regulates pyrimidine nucleotide biosynthesis. The enzyme is inhibited by CTP and can be further inhibited by UTP, although UTP alone has little or no influence on activity; however, the mechanism for the synergistic inhibition is still unknown. In order to determine how UTP is able to synergistically inhibit ATCase in the presence of CTP, we determined a series of X-ray structures of ATCase•nucleotide complexes. Analysis of the X-ray structures revealed that (1) CTP and dCTP bind in a very similar fashion, (2) UTP, in the presence of dCTP or CTP, binds at a site that does not overlap the CTP/dCTP site, (3) the triphosphates of the two nucleotides are parallel to each other with a metal ion, in this case Mg^{2+}, coordinated between the β and γ phosphates of the two nucleotides. Kinetic experiments showed that the presence of a metal ion such as Mg^{2+} is required for synergistic inhibition. Together these results explain how the binding of UTP can enhance the binding of CTP and why UTP binds more tightly in the presence of CTP. A mechanism for the synergistic inhibition of ATCase is proposed in which the presence of UTP stabilizes the T state even more than CTP alone. These results also call into question many of the past kinetic and binding experiments of ATCase with nucleotides as the presence of metal contamination was not considered important.

Keywords

pyrimidine nucleotide biosynthesis; feedback inhibition; allostery; X-ray crystallography

The enzyme aspartate transcarbamoylase (aspartate carbamoyltransferase, ATCase, EC 2.1.3.2) from *Escherichia coli* catalyzes the committed step in pyrimidine nucleotide biosynthesis and allosterically regulates the pathway. Allosteric regulation is critical in the overall control of many metabolic pathways as the specific needs of the cell are fulfilled by modulating the flux through the pathway. *E. coli* ATCase has been extensively studied and has become a classic model of allosteric regulation.[1] Kinetic studies have shown that the enzyme is inhibited by CTP, activated by ATP,[2] and synergistically inhibited by UTP in the presence of CTP.[3] The kinetic response of the enzyme to these effectors helps to maintain a balanced pool of pyrimidine and purine nucleotides in the cell.

The *E. coli* ATCase holoenzyme is a dodecamer composed of six regulatory chains and six catalytic chains arranged into three regulatory dimers and two catalytic trimers. The catalytic chains are responsible for enzyme activity while the regulatory chains bind the allosteric effectors. Each regulatory chain is composed of two separate folding domains, the allosteric domain, responsible for binding the nucleotide effectors, and the zinc domain, responsible for the binding of a structural zinc ion. Each catalytic chain is also composed of two separate

*evan.kantrowitz@bc.edu, Tel. (617)-552-4558.

folding domains, the CP domain, responsible for binding of carbamoyl phosphate, and the Asp domain, responsible for binding of Asp.

ATCase exists in two states: a low-activity, low-affinity for the substrates T state, and a high-activity, high-affinity for the substrates R state. These two states differ in both tertiary and quaternary structures. Each of the substrates and the allosteric effectors have an effect on the T to R equilibrium.[4]

Structural and kinetic data have shown that ATP and CTP compete for and bind to the same site in the allosteric domain, but exhibit opposite effects on ATCase activity.[5] Binding experiments with the holoenzyme have shown that both ATP and CTP exhibit three high-affinity and three low-affinity sites,[6] and binding experiments with the isolated regulatory dimer have shown one high-affinity and one low-affinity site per dimer.[6] UTP alone binds but does not inhibit the enzyme unless CTP is present.[7] Upon the addition of UTP, the number of CTP binding sites decreases from six to three suggesting that CTP is binding to the high-affinity sites and UTP is binding to the low-affinity sites.[8]

The binding of nucleotides to the allosteric sites has also been investigated by the incorporation of the non-natural fluorescent amino acid L-(7-hydroxycoumarin-4-yl)ethylglycine at position 52 in the regulatory chain and measuring the change in fluorescence intensity of the enzyme as a function of nucleotide concentration.[9] These experiments indicated that CTP binds to the enzyme with the same affinity regardless of the presence of UTP and *vice versa*, suggesting that CTP and UTP do not compete for the same binding site. They concluded by speculating that the two identical allosteric sites on a regulatory dimer were functionally asymmetric.

Understanding the allosteric mechanism of ATCase has proven difficult with many conflicting results, notably the observed asymmetry, and the synergistic inhibition by UTP in the presence of CTP. A recent R-state structure of the ATCase•UTP complex provided an important clue to understand the allosteric regulation of ATCase.[10] UTP was shown to bind to the regulatory chain of ATCase in a position different than previously observed for either ATP or CTP (Fig. 1). Peterson *et al.*[10] proposed that each regulatory chain consists of two adjacent but not overlapping binding sites, the A and B sites, with ATP and CTP binding in the A site and UTP binding in the B site. In order to determine how UTP is able to synergistically inhibit ATCase in the presence of CTP, we determined a series of X-ray structures of ATCase•nucleotide complexes including the structures of ATCase•dCTP, ATCase•CTP, ATCase•dCTP•UTP, ATCase•dCTP•UTP•Mg^{2+} and ATCase•CTP•UTP•Mg^{2+}. By showing that dCTP and CTP bind in essentially the same manner to ATCase, and that UTP can synergistically inhibit ATCase in the presence of dCTP in kinetic experiments, we were able to use dCTP as a surrogate for CTP in the structural studies. The use of dCTP as a functional and structural analogue of CTP allowed us to distinguish the nucleotide bound in the A and B sites of the enzyme. These structures provide the critical information necessary for the formulation of a new mechanism of allostery for ATCase.

MATERIALS AND METHODS

Enzyme expression and purification

E. coli ATCase was overexpressed in M9 media supplemented with 5 g/L casamino acids using *E. coli* strain EK1104[11] *[F⁻ ara, thi, Δ(pro-lac), ΔpyrB, pyrF±, rpsL]* transformed with plasmid pEK152[12] containing the *E. coli pyrBI* gene. The isolation and purification procedures were modified versions of those previously described.[11] The first step was ion-exchange chromatography using a Q-Sepharose Fast Flow column (11 cm × 2.5 cm; GE

Healthcare). The protein was eluted with a linear gradient of 0.05 M Tris-acetate and 2 mM 2-mercaptoethanol, pH 8.3 (Low Q buffer) to Low Q buffer containing 0.5 M NaCl (0.4%/min, 250 mL total) at a flow rate of 1.0 mL/min. The fractions containing ATCase were pooled and dialyzed against Low Q buffer. The protein solution was then brought to 20% ammonium sulfate saturation and purified by hydrophobic interaction chromatography using a Phenyl Sepharose column (8.5 cm × 2 cm, GE Healthcare). The protein was eluted using a linear gradient from Low Q buffer brought to 20% ammonium sulfate saturation to Low Q buffer (0.5%/min, 200 mL total) at a flow rate of 1.0 mL/min. The fractions containing pure ATCase, determined by SDS-PAGE,[13] were pooled and dialyzed against 40 mM KH_2PO_4, 2 mM 2-mercaptoethanol, 2 mM EDTA, pH 7.0. Enzyme concentrations were determined by absorbance measurements at 280 nm with an extinction coefficient of 0.59 cm^2/mg.[14]

Determination of ATCase activity

ATCase activity measurements were determined colorimetrically in 20 mM bis-Tris, 20 mM Tris, 20 mM CAPS buffer, pH 7.0 at 25° C, in the presence of a 5.0 mM L-aspartate and a saturating concentration of carbamoyl phosphate (2.4 mM).[15] Kinetic measurements were determined in duplicate, and the data points in the graphs are the average. Nucleotide inhibition curves were determined at the $[Asp]_{0.5}$ (5 mM). Prior to use, nucleotide solutions were treated with chelating ion-exchange resin (Chelex 100, Bio-Rad) to remove trace divalent metals. The resin was directly added to the solutions (0.5 g per 10 mL of nucleotide solution) and stirred on ice for one hour. Following centrifugation, the solution was decanted from the resin. Nucleotide concentrations were determined by absorbance measurements at 271 nm (ε = 9000 $M^{-1}cm^{-1}$, pH = 7.0) for CTP and dCTP and at 262 nm (ε = 10,000 $M^{-1}cm^{-1}$, pH = 7.0) for UTP.[16] For inhibition curves with CTP or dCTP and UTP, $MgCl_2$ was added to an aliquot of the de-metaled UTP solution in a 1:1 molar ratio. Fitting of the experimental data to theoretical equations was accomplished by nonlinear regression.

Crystallization, X-ray data collection, and processing

E. coli ATCase (20 mg/mL) was placed in four 50 μL dialysis buttons (Hampton Research, Aliso Viejo, CA) and dialyzed against 20 mL of crystallization buffer (40 mM sodium citrate, 1 mM 2-mercaptoethanol, 0.2 mM EDTA,1.0 mM CTP, pH 5.7) at 20°C. Crystals formed in about 1 week. One dialysis button was transferred to 2 mL of crystallization buffer with 5 mM UTP and 5 mM $MgCl_2$ and allowed to equilibrate for 12 hours. *E. coli* ATCase was co-crystallized with dCTP following the same procedure as indicated above, but dCTP was substituted for CTP in the crystallization buffer. Crystals formed in about 1 week and one button was dialyzed in crystallization buffer containing 5 mM UTP and 5 mM $MgCl_2$ for 12 hours.

After equilibration in crystallization buffer with 5 mM UTP and 5 mM Mg^{2+}, the crystals were transferred into a cryoprotectant of 20% 2-methyl-2,4-pentadiol in UTP•Mg^{2+} crystallization buffer for about 1 min prior to freezing in liquid nitrogen. Data were collected on beamline X29 at the National Synchrotron Light Source at Brookhaven National Laboratory (Upton, NY) with the exception of the ATCase•CTP data, which were collected on a Rigaku MicroMax-07 HF high intensity microfocus rotating Cu anode X-ray generator coupled with Osmic VariMax Optics and a R-Axis IV++ image plate area detector. The diffraction data were integrated, scaled, and averaged using HKL2000.[17] Data collection and refinement statistics are shown in Table 1.

Structure solution and data refinement

Each structure was directly solved using the coordinates for *E. coli* ATCase in the T state with CTP bound (PDB ID: 1ZA1)[18] as the initial model, after removal of water and ligand molecules. Automated refinements using translation libration screw-motion (TLS)

parameters were performed in PHENIX.[19] Manual rebuilding, addition of waters, and nucleotide modeling were performed using COOT.[20, 21] Waters were accepted if they were within hydrogen-bonding distance of main-chain or side-chain atoms. The final structures were validated using MolProbity[19] and PROCHECK.[22] Coordinates and structure factors for the ATCase•dCTP, ATCase•CTP, ATCase•dCTP•UTP•Mg^{2+}, and ATCase•CTP•UTP•Mg^{2+} complexes have been deposited in the Protein Data Bank under accession codes 4FYV, 4FYW, 4FYX, and 4FYY respectively.

RESULTS AND DISCUSSION

Structural data of ATCase with only CTP bound[18] or only UTP bound[10] does not clarify how the two nucleotides synergistically inhibit ATCase. A single structure of the enzyme with both nucleotides bound is needed to definitively determine the mode of UTP binding to the enzyme in the presence of CTP and would help to elucidate the mechanism of the synergistic inhibition. However, at a resolution of ~2 Å the electron density profiles for CTP and UTP are virtually indistinguishable. Therefore, we sought a functional analogue of CTP with an altered electron density profile that still retained UTP synergic inhibition. Previous studies have shown that dCTP inhibits ATCase to approximately the same extent as CTP,[23] suggesting that the 2′-hydroxyl group is not important for allosteric inhibition of ATCase. UTP does function as a synergistic inhibitor in the presence of dCTP. As seen in Fig. 2, at 2 mM dCTP inhibits the enzyme 67% as compared to 43% for CTP. The combination of 2 mM dCTP and 2 mM UTP inhibits the enzyme 93% as compared to 86% for 2 mM CTP and 2 mM UTP. The ability of UTP to synergistically inhibit ATCase in combination with either dCTP or CTP allowed us to use dCTP as a surrogate of CTP in the structure determination.

Comparison of the ATCase•dCTP and ATCase•CTP structures

To further validate the use of dCTP as a substitute for CTP, the structures of the ATCase•dCTP and ATCase•CTP complexes were determined. Identical conditions were used to co-crystallize the enzyme with either dCTP or CTP. Both complexes crystallized in the P321 space group with almost identical unit cell dimensions (Table 1), and in both cases data were collected to a resolution limit of 2.1 Å. The structure of the ATCase•CTP complex determined here is at a higher resolution than previously reported.[5, 18, 24]

Overall, the ATCase•CTP and ATCase•dCTP structures are very similar with a main-chain RMSD of 0.187 Å. For comparison, the main-chain RMSD between the ATCase•CTP complex previously determined (PDB ID 1ZA1) and the structure of the same complex reported here is 0.221 Å. Both CTP and dCTP bind in the A site of the regulatory chain (Fig. 1), as defined by Peterson *et al.*[10] and bind with identical interactions with the exception of the one involving the 2′-hydroxyl of CTP (Fig. 3). The binding site includes two Lys residues; Lys94 interacts with the phosphates of the nucleotide, and Lys60 interacts with the 2-keto group on the cytosine ring. Backbone atoms of Tyr89 and Ile12 also make polar interactions with the cytosine ring and His20 and Asp19 interact with the γ-phosphate and the 3′-hydroxyl group, respectively. There are also several residues that contribute to the binding via hydrophobic interactions including Ile12, Val17, Leu58, Ile86 and Val91.

The binding of dCTP in the r1 and r6 chains is asymmetric. The all-atom RMSD between dCTP in the two chains is 2.28 Å. The position of the cytosine rings in the r1 and r6 chains are nearly identical, however, the ribose triphosphate portion is displaced in the r1 as compared to the r6 chain. This displacement may be due to the loss of an interaction between Lys94 and a γ phosphate oxygen that is observed in the r6 but not in the r1 chain. In fact, there are no interactions between the triphosphate portion of dCTP with the protein in the r1 chain. In the ATCase•CTP complex, the CTP bound in the r1 and r6 chains exhibit very similar interactions, and the all-atom RMSD between CTP in the r1 and r6 chains is

0.269 Å. The all-atom RMSD between dCTP and CTP in the two structures bound in the r1 and r6 chains are 2.39 Å and 0.88 Å, respectively. The higher RSMD in the r1 chain reflects the asymmetry observed between the r1 and r6 chains in the ATCase•dCTP structure mentioned above.

The structure of the ATCase•dCTP•UTP complex

Crystals of the ATCase•dCTP complex were dialyzed against a 5 mM solution of UTP in crystallization buffer for 12 hours before the crystals were dipped in cryoprotectant and frozen for data collection. The previously determined structure of the ATCase•CTP complex (PDB ID 1ZA1)[18] was used as the initial model for structure refinement. This preliminary structure of the ATCase•dCTP•UTP complex suggested that dCTP bound in the A site and UTP bound in the B site on each regulatory chain simultaneously, with their β and γ phosphates essentially parallel to each other. The data also showed excess electron density between the β and γ phosphates up to the 11.0 σ level. This density and its position could be explained by the presence of a metal ion serving to neutralize the repulsion of the negatively charged phosphate oxygens of the dCTP and UTP. The metal ion would thereby assist/stabilize the binding of the two nucleotides to the A and B sites by diminishing the repulsion of the phosphate oxygens and create an additional interaction site for each nucleotide. The buffers used for growth of these crystals contained no added metals so presumably the electron density observed was the result of metal ion contamination in the buffer components or the nucleotide solutions.

The synergistic inhibition of ATCase by CTP and UTP is metal dependent

The preliminary structure of the ATCase•dCTP•UTP complex, discussed above, suggested that a metal ion was coordinated between the β and γ phosphates of the two nucleotides. Previous studies reported the allosteric effectors ATP and CTP are influenced by the presence of Mg^{2+}, presumably due to the formation of the ATP•Mg^{2+} and CTP•Mg^{2+} complexes.[25–27] Honzatko *et al.*[27] tested a variety of metal ions including Al^{3+}, Mg^{2+}, Mn^{2+} and Ca^{2+} and found that Mg^{2+} and Mn^{2+} altered the response of the nucleotides the most. However, the influence of metal ions on the synergistic inhibition of ATCase by UTP in the presence of CTP has not been reported. Since the concentration of Mg^{2+} in *E. coli* cells is approximately 2.5 mM,[28, 29] and the formation of Mg^{2+} nucleotide complexes is well established, the influence of Mg^{2+} on the ability of UTP to synergistically inhibit ATCase in the presence of CTP was measured. For these experiments all nucleotide solutions were de-metaled before use.

As seen in Fig. 4, de-metaled UTP did not synergistically inhibit ATCase in the presence of dCTP or CTP, although, de-metaled CTP or dCTP was able to inhibit the enzyme (see Fig. 2). The inhibition profile was different with UTP•Mg^{2+} (1:1 ratio). UTP•Mg^{2+} was able to inhibit the enzyme in the presence of CTP or dCTP (Fig. 4A,B). Therefore, the metal not only assists in the binding of UTP to the B site when CTP is present, as suggested by the structural data, but also Mg^{2+} is critical in the synergic inhibition of the enzyme. Furthermore, the reported enhanced affinity of UTP in the presence of CTP and *vice versa*[7] can also be explained by the Mg^{2+}, as it would add additional binding loci for each nucleotide when present.

As a control, the influence of Mg^{2+} on the activity of ATCase was determined in the presence of 2 mM dCTP or CTP (Fig. 4). In both cases, the addition of Mg^{2+} increased the activity; however, the extent of the increase was not as large as the decrease induced by the 2 mM dCTP or CTP. One explanation for this increase in activity is the ability of Mg^{2+} to complex with CTP to form CTP•Mg^{2+}. Depending upon the relative affinities of Mg^{2+} and ATCase for CTP, the addition of Mg^{2+} may result in some dissociation of CTP from the

enzyme thereby increasing enzyme activity. This explanation is supported by the results of the experiments in which UTP•Mg^{2+} was added. As seen in Fig. 4, at low concentrations of UTP•Mg^{2+} there is also a small increase in relative activity before the synergistic UTP inhibition is observed. Any free Mg^{2+} may be complexing with enzyme bound CTP.

The structure of the ATCase•dCTP•UTP•Mg^{2+} complex

Since the preliminary structure of the ATCase•dCTP•UTP complex suggested the presence of a metal ion helping to neutralize the charges on the phosphate oxygens, and the fact that the synergistic inhibition is not readily observed in the absence of a divalent metal (e.g. Mg^{2+}), the structure of the ATCase•dCTP•UTP•Mg^{2+} complex was determined. In this study, ATCase•dCTP crystals were dialyzed against crystallization buffer supplemented with 5 mM UTP and 5 mM Mg^{2+}. The structure of the ATCase•dCTP•UTP•Mg^{2+} complex was essentially identical to the preliminary ATCase•dCTP•UTP structure, with the Mg^{2+} clearly visible between the dCTP and UTP.

Fig. 5A shows the $2F_o - F_c$ electron density map of the nucleotides bound to the allosteric site. To verify the assignment of dCTP to the A site and UTP to the B site, electron density maps were generated with UTP modeled in the A site and dCTP modeled in the B site. In the case of UTP, the resulting $F_o - F_c$ electron density map showed significant negative density around the oxygen at the 2′-hydroxyl in the A site (Fig 5B), indicating that the molecule in the A site was dCTP and not UTP. Furthermore, the $F_o - F_c$ electron density map for dCTP bound in the B site (Fig. 5B) exhibited positive density at the 2′ ribose position indicating that the molecule in the B site was UTP and not dCTP.

The interactions observed between the protein and dCTP in the A site (Fig. 6A) of this structure are consistent with previously published crystal structures of the ATCase•CTP complex,[18] as well as the structures of the ATCase•dCTP and ATCase•CTP complexes reported here. As shown in Fig. 6A, UTP binds in the B site and exhibits interactions with N-terminal residues Gln8 and Val9, 50's loop residues Ser50, Gly51, Glu52, and Lys56 and residues His20 and Lys60. The backbone atoms of the N-terminal residues Gln8 and Val9 make hydrogen bonding interactions with uracil and the ribose ring, while the 50's loop residues hydrogen-bond with the triphosphate portion of UTP. Residues His20 and Lys60 are positioned at the interface of the A and B sites and each make contact with both nucleotides. His20 interacts with the γ phosphate on each molecule while Lys60 interacts with the 2-keto group of dCTP and the 4-keto group of UTP (Fig. 6A). In addition to the polar contacts described, there are several hydrophobic interactions that contribute to the binding of UTP in the B site involving Leu7, Leu48, Pro49, and Leu58.

The previously reported structure of the ATCase•UTP complex was crystallized in the presence of N-phosphonoacetyl-L-aspartate (PALA), which stabilizes the enzyme in the R state.[10] The structures reported here are in the absence of PALA and in the T state, based upon the vertical separation between the catalytic subunits. The interactions between the enzyme and UTP in the ATCase•UTP•PALA complex in the r6 chain are identical to those observed in the ATCase•dCTP•UTP•Mg^{2+} complex with the exception of Arg41 from the adjacent regulatory chain. In the structure reported here, Arg41 makes a water mediated interaction with the 3′-ribose oxygen of UTP (Fig. 6A). The most likely reason this interaction is not a direct interaction, as seen in the ATCase•UTP•PALA complex, is the conformational difference of the regulatory dimer between the T and R state structures.

The structure of the ATCase•CTP•UTP•Mg^{2+} complex

Based on the fact that in the ATCase•CTP complex no CTP was observed in the B site, crystals of the ATCase•CTP complex were dialyzed into crystallization buffer containing 5

mM UTP and 5 mM Mg^{2+} for 12 hours in an identical fashion as indicated above for the crystallization of the ATCase•dCTP•UTP•Mg^{2+} complex. Crystals were then cryoprotected and flash frozen before data collection. Although the density of the nucleotides in the A and B sites are nearly identical, CTP was modeled into the A site and UTP was modeled into the B site (Fig. 6B), because of the selective binding observed for dCTP/CTP in the A site and UTP in the B site. All the interactions mentioned above between the enzyme and dCTP and UTP are present in the ATCase•CTP•UTP•Mg^{2+} structure. However, there is an additional polar interaction between the 2′-hydroxyl of CTP and the 4-keto group of UTP. Interestingly, the interaction between Lys60 and the 2′-hydroxyl group observed in the ATCase•CTP complex (Fig. 3) was not present in the ATCase•CTP•UTP•Mg^{2+} complex. As seen in Fig. 7, the Mg^{2+} in the ATCase•CTP•UTP•Mg^{2+} complex exhibits square bipyramidal geometry with all oxygen ligands. The oxygens in the four equatorial positions are donated by β and γ phosphate oxygens of both CTP and UTP, while the axial positions are both donated from oxygens of water molecules. Hydrogen bonding interactions that the Mg^{2+} creates, between the side chains of Asp19, His20 and the phosphate oxygens add to the interactions between the two nucleotides.

These structural and kinetic results call into question many of the previously reported binding and kinetic studies involving the function of the allosteric effectors on ATCase, as these studies did not take into account metal ion contamination. Steps to control metal ion contamination prior to binding and kinetic experiments with ATCase should be taken to ensure that the allosteric response of the enzyme corresponds to what are most likely the conditions in the cell.

Nucleotide binding site specificity

X-ray structures of the ATCase•CTP and the ATCase•UTP[10] complexes showed that CTP and UTP bind at close but not overlapping sites in the allosteric domain (see Fig. 1). Fig. 8 shows the electrostatic potential of the protein, calculated using Delphi,[30] mapped onto the surface. The entire nucleotide binding site exhibits an overall positive electrostatic potential, which would enhance the binding of the triphosphate portion of the nucleotides in the A and B sites.

The specificity of CTP for the A site is related to the electrostatic and hydrogen bonding interactions with the cytosine ring. The most positive portion of the binding site, corresponding to Lys60, interacts with the 4-keto group of UTP, and the 2-keto of CTP, which have negative partial atomic charges. In the A site, the 4-amino group of CTP with a partial atomic charge of +0.4, as calculated using Jaguar (Schrödinger, Inc.), interacts with the backbone oxygen atoms of Tyr89 and Ile12, which have partial atomic charges of −0.6 and −0.5 respectively. If UTP were to bind in the A site, there would be no hydrogen bonding donors to form interactions with Ile12 and Tyr89 suggesting that UTP would have diminished affinity for the A site as compared to the B site.

The specificity of UTP for the B site is related to the electrostatic and hydrogen bonding interactions with the uracil ring. In the B site, the 2-keto group and the hydrogen on the 3 nitrogen of UTP, interact with the backbone nitrogen and oxygen atoms of Val9. In addition, the 4-keto group interacts with the ε-amino group of Lys60 and the 2′-hydroxyl of CTP. If CTP were to bind in the B site the interactions with Val9 would still be possible, however, the +0.4 partial atomic charge on the 4-amino group would result in a repulsive interaction with Lys60, thus significantly reducing the affinity for CTP to the B site.

Conformational changes due to nucleotide binding

A comparison of the ATCase•CTP•UTP•Mg^{2+} structure to a T-state structure in the absence of nucleotides (PDB ID 1NBE)[31] indicates that the largest conformational changes are observed at the N-terminus and the 50's loop in the allosteric domain and the 120's and 130's loops in the zinc domain. The conformational differences in the N-termini are most likely due to the mobility of these regions, which is reflected in weak electron density. For this reason, between 5 and 9 residues were not included in the deposited coordinates. As Peterson *et al.*[10] previously observed in the ATCase•UTP structure, the 50's loop is perturbed upon UTP binding as this loop has a number of interactions with the nucleotide. The 120's loop, a loop remote from the nucleotide binding site but in close proximity to the regulatory-catalytic chain interface, undergoes structural alterations upon nucleotide binding. This displacement of the 120's loop may propagate to the CP domain of the catalytic chain via the regulatory-catalytic chain interface.

The structures of the ATCase•dCTP•UTP•Mg^{2+} and ATCase•dCTP•UTP•Mg^{2+} complexes explain results of previous mutagenesis studies

The discovery that UTP binds to the B site of each regulatory chain explains previous kinetic results observed for many single amino acid substitution mutants of ATCase that result in the loss of the ability of UTP to inhibit catalysis in the presence of CTP. Until now the reasons why regulatory mutants K56A,[32] K60A,[33] H20A,[34] D19A,[35] K6A[36] and L7A[36] did not exhibit UTP synergistic inhibition were not known. From this work, the side chains of Asp19, His20 and Lys60 interact with both CTP and UTP. The lack of synergistic inhibition previously reported but not wholly understood at the time is most likely due to reduced affinity of both CTP and UTP. In the case of the D19A mutation, the binding of UTP in the presence of CTP could not be detected.[35] Both Lys6 and Leu7 were shown by crystallography to be involved in the binding of UTP in the B site, and the loss of these stabilizing interactions can explain why the mutant enzymes do not exhibit synergistic inhibition. The salt link between Lys56 and UTP explains the loss of synergistic inhibition, when Lys56 is replaced by alanine.

While it is clear that these mutant enzymes would show diminished synergistic effects because of the reasons mentioned above, the kinetic studies on all of the mutant enzymes involved in CTP and UTP binding can be questioned, because of the metal ion site between the nucleotides. Kinetic experiments in this study showed that removal of trace metals in the nucleotide solutions resulted in no synergistic effect. In previous studies showing synergistic inhibition of UTP in the presence of CTP, it is most likely that there were sufficient amounts of metal ion contamination to induce the effect. Since the intracellular concentrations of metals such as Mg^{2+} are significant, metal ion involvement in the allosteric regulation of ATCase is certain.

Mechanism of the synergistic inhibition of ATCase by UTP in the presence of CTP

Based upon the results reported here and previous studies we know: (1) CTP alone binds to the enzyme and causes inhibition, (2) Mg^{2+} has only a small influence on the inhibition of the enzyme by CTP, (3) UTP alone binds to the enzyme but does not cause inhibition[3, 10], (4) Mg^{2+} is required for the synergistic inhibition of the enzyme by UTP in the presence of CTP, and (5) CTP and UTP bind at distinct sites on the regulatory chain that are not overlapping. The crystal structures of the ATCase•dCTP•UTP•Mg^{2+} and ATCase•CTP•UTP•Mg^{2+} complexes, along with these experimental results, allow us to propose a mechanism for the synergistic inhibition of ATCase by UTP in the presence of CTP.

The binding of CTP to the allosteric "A site"[10] induces conformational changes within the enzyme resulting in a stabilization of the T state. In the absence of CTP the [T]/[R] ratio is about 250 which increases to about 1250 in the presence of CTP.[4] This shift in the [T]/[R] ratio explains the observed shift to the right in the aspartate saturating curve in the presence of CTP, and the decrease in enzyme activity at a fixed concentration of aspartate. The fact that UTP can bind to the allosteric "B site" in the absence of metals[10], but does not influence the activity of the enzyme[3], indicates that the binding of UTP alone does not stabilize the T or R states of the enzyme. However, under physiological conditions it is unlikely that UTP would not be complexed with Mg^{2+}. The structures of ATCase•dCTP•UTP•Mg^{2+} and ATCase•CTP•UTP•Mg^{2+} both support a model in which the two nucleotides act together in a combined AB allosteric site. However, a combined allosteric response is only elicited if CTP is bound to the A site and UTP•Mg^{2+} is bound to the B site. The role of the Mg^{2+} is essentially to allow both nucleotides to bind simultaneously, as the repulsion of their negatively charged phosphates would preclude their simultaneously binding. Since the binding of UTP alone to the enzyme in the B site elicits no inhibitory response, we propose that the AB allosteric site, where the two nucleotides are linked by a metal ion allows UTP to amplify the kinetic response of the CTP bound in the A site. Thus, the ATCase•CTP•UTP•Mg^{2+} complex stabilizes the T state more than CTP alone, shifts the aspartate saturating curve to the right more than CTP alone,[3] and the activity of the enzyme is even more reduced than CTP alone at a fixed concentration of aspartate.[3]

Previous studies suggested that the role of the B site to amplify or modify the functional effect of the nucleotide in the A site is not restricted to just the synergistic inhibition of UTP in the presence of CTP. For example, Kleppe and Spaeren[25] first observed that Mg^{2+} altered the response of the enzyme for ATP. Detailed kinetic and small-angle X-ray scattering experiments[37] showed that ATP•Mg^{2+} could stimulate the activity of ATCase almost twice as much as ATP in the absence of Mg^{2+}. The enhanced stimulation of the enzyme by ATP•Mg^{2+} may be explained by the simultaneous binding of two ATP molecules to the AB allosteric site bridged by a Mg^{2+}. Again in this case the B site nucleotide, here ATP, would amplify the response of the ATP in the A site. ATP alone shifts the [T]/[R] ratio from 250 to about 70. The combined binding of ATP•Mg^{2+}•ATP in the allosteric site could stabilize the R state even more than ATP alone and reduce the [T]/[R] ratio even more. This change in the [T]/[R] ratio would shift the aspartate saturating curve to the left such that at a fixed concentration of aspartate, the binding of ATP•Mg^{2+}•ATP at the allosteric site would stimulate the enzyme more than ATP alone. In addition, Honzatko *et al.*[27] reported that GTP•Mg^{2+} had a larger influence on ATCase activity than GTP alone. It is clear that the role of a metal cation in the allosteric regulation of ATCase has been underestimated. Furthermore, the data from many previous studies are now essentially impossible to interpret correctly as the extent of metal ion contamination is unknown. A reevaluation of nucleotide effects on ATCase is now required with emphasis on nucleotide combinations in the presence of physiological levels of metal cations.

Rational for the synergistic inhibition of ATCase by UTP in the presence of CTP

As pointed out by Wild *et al.*[3], high concentrations of CTP not only feedback inhibit ATCase, but also inhibit CTP synthetase by competitive inhibition of its own synthesis.[38] A possible result of the inhibition of CTP synthetase would be to elevate levels of UTP. The synergistic feedback inhibition of ATCase by UTP in the presence of CTP would therefore act to modulate the biosynthesis of UTP as well as CTP. However, if cellular levels of UTP were low, the synergistic feedback inhibition of ATCase by UTP would not occur allowing for higher levels of pyrimidine nucleotide biosynthesis resulting in elevated levels of UTP.

Conclusions

Although there have been many binding and kinetic studies measuring the affinity and functional consequences of nucleotide binding at the allosteric sites of ATCase, discrepancies between these studies have hindered the development of a consistent mechanism for allosteric regulation in ATCase. The findings in this work provide two new facts that need to be reconciled with all of the previous experimental data. First, the allosteric site on each regulatory chain of ATCase can bind two nucleotide triphosphates simultaneously, in adjacent but not overlapping sites. Second, a metal ion, Mg^{2+} in these studies, is required for the nucleotide in the B site to function and perhaps for binding as well. In the case of the synergistic inhibition of ATCase by UTP in the presence of CTP, it is the UTP•Mg^{2+} bound in the B site that enhances the inhibition of CTP. UTP alone does not inhibit the enzyme, since the A site has a preference for cytosine rather than a uracil base. Furthermore, UTP does not enhance the CTP inhibition without Mg^{2+}. Since Mg^{2+} is known to enhance the allosteric activation of the enzyme by ATP it is more than likely that the AB allosteric site of ATCase can accommodate ATP•Mg^{2+}•ATP in a similar fashion as has been shown here for CTP•Mg^{2+}•UTP. New structural and functional studies of ATCase are required to probe the allosteric response of the enzyme in the presence of nucleotides and metal ions, conditions that would be more physiologically relevant than those used in previous studies.

Acknowledgments

We thank Howard Robinson of Brookhaven National Laboratory for data collection and assistance with data processing.

Funding Sources

This work was supported by Grant GM26237 from the National Institutes of Heath. Use of the National Synchrotron Light Source, Brookhaven National Laboratory, was supported by the U.S. Department of Energy, Office of Science, Office of Basic Energy Sciences, under Contract No. DE-AC02-98CH10886.

ABBREVIATIONS

ATCase	aspartate transcarbamoylase
CP	carbamoyl phosphate
RMSD	root mean square deviation
PALA	N-phosphonoacetyl-L-aspartate
50's loop	residues 46–58 of the regulatory chain
120's loop	residues 118–124 of the regulatory chain
130's loop	residues 129–134 of the regulatory chain
c1 and c6	catalytic chains in the asymmetric unit
r1 and r6	regulatory chains of a dimer in the asymmetric unit

References

1. Lipscomb WN, Kantrowitz ER. Structure and mechanisms of *Escherichia coli* aspartate transcarbamoylase. Acc Chem Res. 2012; 45:444–453. [PubMed: 22011033]
2. Gerhart JC, Pardee AB. The effect of the feedback Inhibitor CTP, on subunit interactions in aspartate transcarbamylase. Cold Spring Harbor Symp Quant Biol. 1963; 28:491–496.

3. Wild JR, Loughrey-Chen SJ, Corder TS. In the presence of CTP, UTP becomes an allosteric inhibitor of aspartate transcarbamylase. Proc Natl Acad Sci U S A. 1989; 86:46–50. [PubMed: 2643106]
4. Howlett GJ, Blackburn MN, Compton JG, Schachman HK. Allosteric regulation of aspartate transcarbamoylase. Analysis of the structural and functional behavior in terms of a two-state model. Biochemistry. 1977; 16:5091–5099. [PubMed: 334257]
5. Stevens RC, Gouaux JE, Lipscomb WN. Structural consequences of effector binding to the T state of aspartate carbamoyltransferase: Crystal structures of the unligated and ATP- and CTP-complexed enzymes at 2.6 Å Resolution. Biochemistry. 1990; 29:7691–7701. [PubMed: 2271528]
6. Suter P, Rosenbusch JP. Asymmetry of binding and physical assignments of CTP and ATP sites in aspartate transcarbamoylase. J Biol Chem. 1977; 252:8136–8141. [PubMed: 334776]
7. England P, Hervé G. Synergistic Inhibition of *Escherichia coli* Aspartate Transcarbamoylase by CTP and UTP: Binding Studies Using Continuous-Flow Dialysis. Biochemistry. 1992; 31:9725–9732. [PubMed: 1390749]
8. Fetler L, Tauc P, Herve G, Cunin R, Brochon JC. Tryptophan residues at subunit interfaces used as fluorescence probes to investigate homotropic and heterotropic regulation of aspartate transcarbamylase. Biochemistry. 2001; 40:8773–8782. [PubMed: 11467937]
9. Mendes KR, Martinez JA, Kantrowitz ER. Asymmetric allosteric signaling in aspartate transcarbamoylase. ACS Chem Biol. 2010; 5:499–506. [PubMed: 20210358]
10. Peterson AW, Cockrell GM, Kantrowitz ER. A second allosteric site in *E. coli* aspartate transcarbamoylase. Biochemistry. 2012; 51:4776–4778. [PubMed: 22667327]
11. Nowlan SF, Kantrowitz ER. Superproduction and rapid purification of *E. coli* aspartate transcarbamoylase and its catalytic subunit under extreme derepression of the pyrimidine pathway. J Biol Chem. 1985; 260:14712–14716. [PubMed: 3902838]
12. Baker DP, Kantrowitz ER. The conserved residues glutamate-37, aspartate-100 and arginine-269 are important for the structural stabilization of *Escherichia coli* aspartate transcarbamoylase. Biochemistry. 1993; 32:10150–10158. [PubMed: 8104480]
13. Laemmli UK. Cleavage of structural proteins during the assembly of the head of bacteriophage T4. Nature. 1970; 227:680–685. [PubMed: 5432063]
14. Gerhart JC, Holoubek H. The purification of aspartate transcarbamylase of *Escherichia coli* and separation of its protein subunits. J Biol Chem. 1967; 242:2886–2892. [PubMed: 5338508]
15. Pastra-Landis SC, Foote J, Kantrowitz ER. An improved colorimetric assay for aspartate and ornithine transcarbamylases. Anal Biochem. 1981; 118:358–363. [PubMed: 7337232]
16. Bock RM, Ling NS, Morell SA, Lipton SH. Ultraviolet absorption spectra of adenosine-5′-triphosphate and related 5′-ribonucleotides. Arch Biochem Biophys. 1956; 62:253–264. [PubMed: 13328113]
17. Otwinowski, Z.; Minor, W. Processing of X-ray diffraction data collected in oscillation mode. In: Carter, CW., Jr; Sweet, RM., editors. Methods Enzymol. Academic Press; NY: 1997. p. 307-326.
18. Wang J, Stieglitz KA, Cardia JP, Kantrowitz ER. Structural basis for ordered substrate binding and cooperativity in aspartate transcarbamoylase. Proc Natl Acad Sci U S A. 2005; 102:8881–8886. [PubMed: 15951418]
19. Adams PD, Afonine PV, Bunkóczi G, Chen VB, Davis IW, Echols N, Headd JJ, Hung L-W, Kapral GJ, Grosse-Kunstleve RW, McCoy AJ, Moriarty NW, Oeffner R, Read RJ, Richardson DC, Richardson JS, Terwilliger TC, Zwart PH. PHENIX: a comprehensive Python-based system for macromolecular structure solution. Acta Cryst. 2010; D66:213–221.
20. Emsley P, Cowtan K. Coot: model-building tools for molecular graphics. Acta Cryst. 2004; D60:2126–2132.
21. Emsley P, Lohkamp B, Scott WG, Cowtan K. Features and Development of Coot. Acta Cryst. 2010; D66:486–501.
22. Laskowski RA, MacArthur MW, Moss DS, Thornton JM. PROCHECK: A program to check the stereochemical quality of protein structures. J Appl Cryst. 1993; 26:283–291.
23. Gerhart JC, Pardee AB. Enzymology of control by feedback inhibition. J Biol Chem. 1962; 237:891–896. [PubMed: 13897943]

24. Kosman RP, Gouaux JE, Lipscomb WN. Crystal structure of CTP-ligated T state aspartate transcarbamoylase at 2.5 Å resolution: Implications for aspartate transcarbamoylase mutants and the mechanism of negative cooperativity. Proteins: Struct Funct Genet. 1993; 15:147–176. [PubMed: 8441751]
25. Kleppe K, Spaeren U. Aspartate transcarbamylase from *Escherichia coli II* Interaction of metal ions with substrates, inhibitors and activators. Biochim Biophys Acta. 1966; 128:199–202. [PubMed: 5339597]
26. Christopherson RI, Finch LR. Regulation of aspartate carbamoyltransferase of *Escherichia coli* by the interrelationship of magnesium and nucleotides. Biochim Biophys Acta. 1977; 481:80–85. [PubMed: 321032]
27. Honzatko RB, Lauritzen AM, Lipscomb WN. Metal cation influence on activity and regulation of aspartate carbamoyltransferase. Proc Natl Acad Sci U S A. 1981; 78:898–902. [PubMed: 7015335]
28. Kung FC, Raymond J, Glaser DA. Metal ion content of *Escherichia coli* versus cell age. J Bacteriol. 1976; 126:1089–1095. [PubMed: 780340]
29. Lusk JE, Williams RJ, Kennedy EP. Magnesium and the growth of *Escherichia coli*. J Biol Chem. 1968; 243:2618–2624. [PubMed: 4968384]
30. Gilson MK, Honig B. Calculation of the total electrostatic energy of a macromolecular system: solvation energies, binding energies, and conformational analysis. Proteins. 1988; 4:7–18. [PubMed: 3186692]
31. Williams MK, Stec B, Kantrowitz ER. A single mutation in the regulatory chain of *Escherichia coli* aspartate transcarbamoylase is an extreme T-state structure. J Mol Biol. 1998; 281:121–134. [PubMed: 9680480]
32. Corder TS, Wild JR. Discrimination between nucleotide effector responses of aspartate transcarbamoylase due to a singe site substitution in the allosteric binding sIte. J Biol Chem. 1989; 264:7425–7430. [PubMed: 2651439]
33. Zhang Y, Kantrowitz ER. Lysine-60 in the regulatory chain of *Escherichia coli* aspartate transcarbamylase is important for the discrimination between CTP and ATP. Biochemistry. 1989; 28:7313–7318. [PubMed: 2510822]
34. Zhang Y, Kantrowitz ER. Probing the regulatory site of *Escherichia coli* aspartate transcarbamoylase by site-specific mutagenesis. Biochemistry. 1992; 31:792–798. [PubMed: 1731936]
35. Zhang Y, Kantrowitz ER. The synergistic inhibition of *Escherichia coli* aspartate carbamoyltransferase by UTP in the presence of CTP is due to the binding of UTP to the low affinity CTP sites. J Biol Chem. 1991; 266:22154–22158. [PubMed: 1939236]
36. Dembowski NJ, Kantrowitz ER. The use of alanine scanning mutagenesis to determine the role of the amino terminus of the regulatory chain in the heterotropic mechanism of *Escherichia coli* aspartate transcarbamoylase. Protein Eng. 1994; 7:673–679. [PubMed: 8073037]
37. Fetler L, Vachette P. The allosteric activator Mg-ATP modifies the quaternary structure of the R-state of *Escherichia coli* aspartate transcarbamylase without altering the TR equilibrium. J Mol Biol. 2001; 309:817–832. [PubMed: 11397099]
38. Long CW, Pardee AB. Cytidine triphosphate synthetase of *Escherichia coli B* I Purification and kinetics. J Biol Chem. 1967; 242:4715–4721. [PubMed: 4862983]

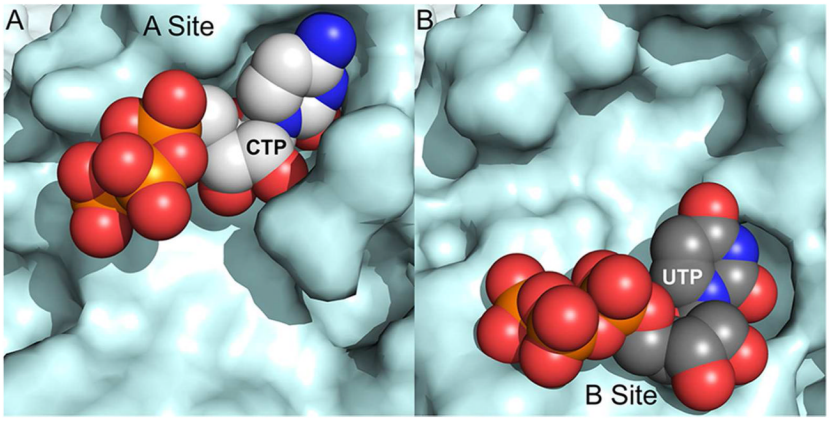

Figure 1.

The (A) CTP and (B) UTP binding sites in ATCase. The r6 regulatory chain of the ATCase•CTP structure (PDB ID 8AT1) and the ATCase•UTP structure (PDB ID 4F04) are shown from the same viewpoint. The allosteric sites are shown in a surface representation with the nucleotide shown as CPK.

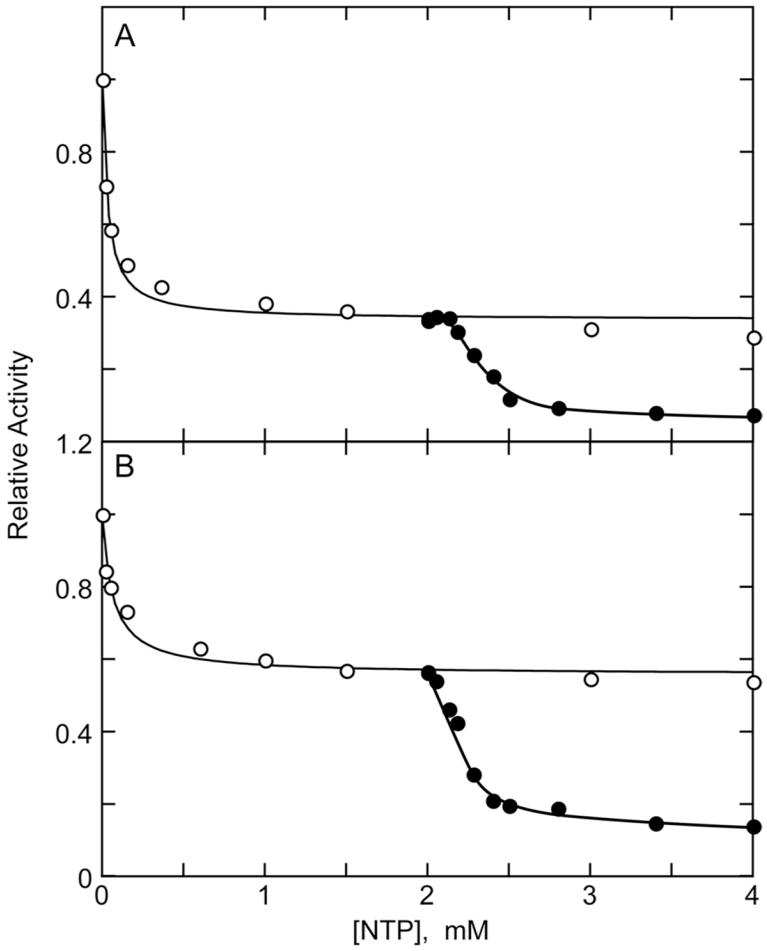

Figure 2.

Influence of nucleotides on the activity of ATCase. Relative activity was measured at increasing concentrations of nucleotide (NTP). When UTP and CTP or dCTP were present simultaneously, the abscissa corresponds to the total nucleotide concentration. (A) Influence on activity of dCTP alone (○) and of dCTP plus UTP•Mg^{2+} (●). When the concentration of dCTP reached 2 mM, UTP•Mg^{2+} was added. The UTP•Mg^{2+} concentration was increased from 0 to 2 mM while the concentration of dCTP remained constant (2 mM). (B) Identical experiment as depicted in (A) using CTP in place of dCTP.

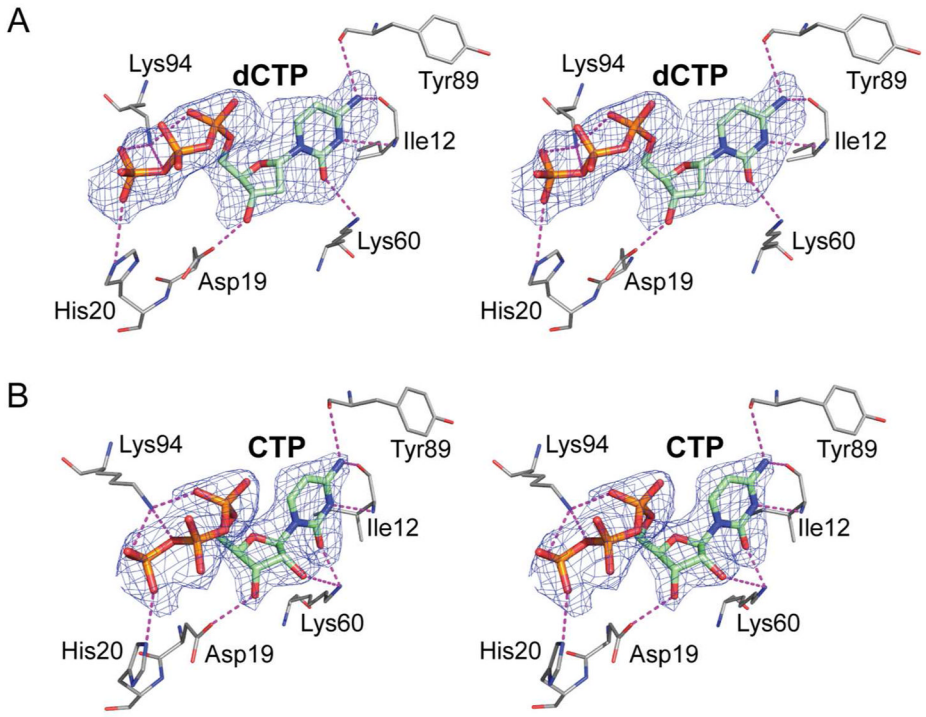

Figure 3.

Stereoview of the r6 regulatory site of ATCase shown with (A) dCTP and (B) CTP bound. Polar interactions are indicated with dashed lines. Simple $F_o - F_c$ omit electron density maps are shown at 3.0 σ. For these maps the nucleotides were omitted from the calculations.

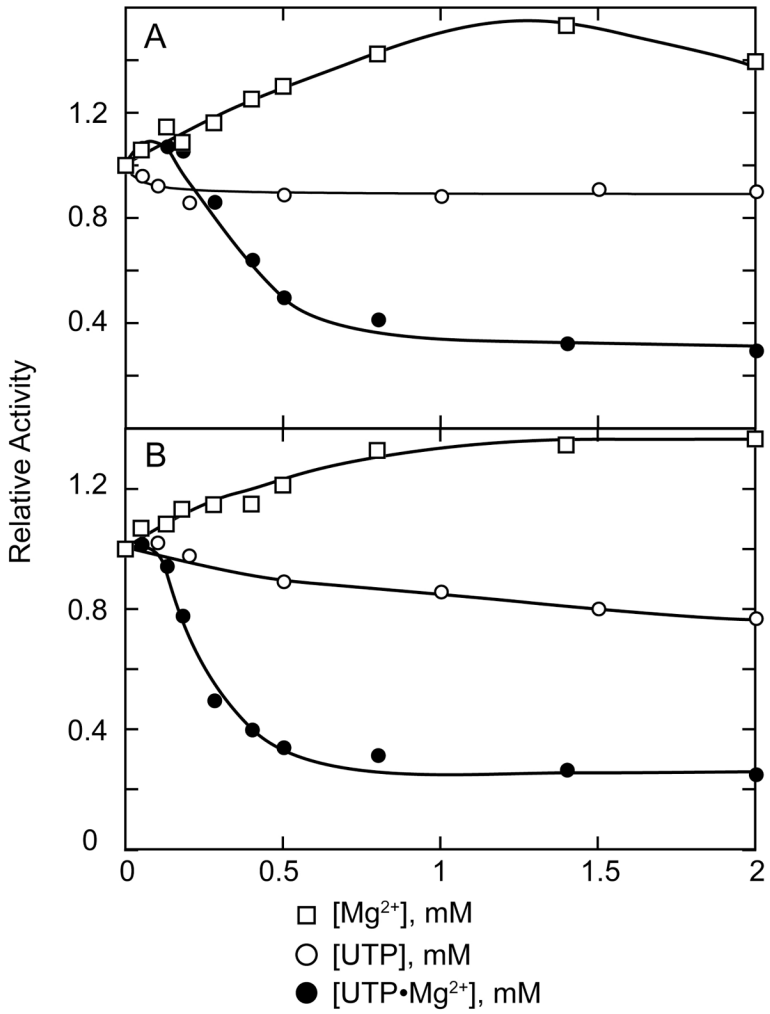

Figure 4.

Influence of Mg^{2+}, UTP and UTP•Mg^{2+} on ATCase activity. Each data point was determined in duplicate, and the data points shown are the average. Relative activity was measured in the presence of either 2 mM (A) dCTP or (B) CTP with increasing concentrations of Mg^{2+} (□), UTP (○) and UTP•Mg^{2+} (●).

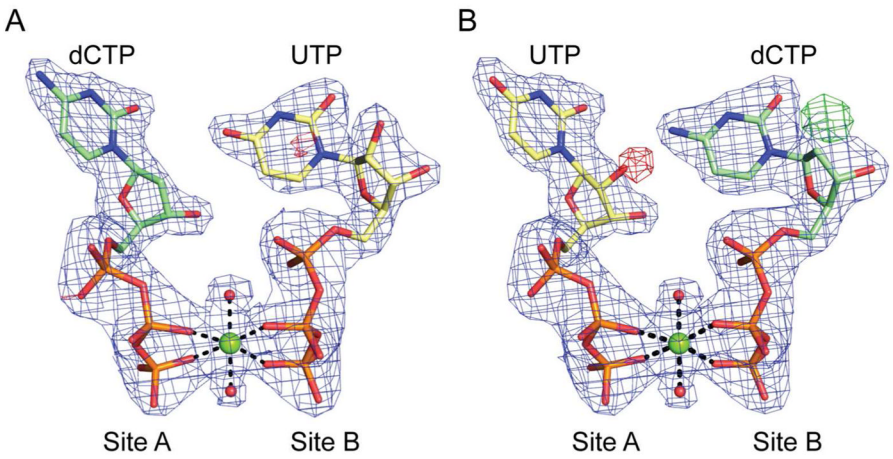

Figure 5.

The allosteric site of ATCase showing the A and B sub-sites. (A) Mg^{2+} (green sphere) is coordinated to β and γ phosphates of both dCTP (green carbons) and UTP (yellow carbons) and two water molecules. (B) Modeling of UTP in the A site and dCTP in the B site. Shown in both (A) and (B) are the $2F_o - F_c$ (blue, 1.5 σ) and $F_o - F_c$ (green, 5.0 σ, and red, −3.5 σ) electron density maps.

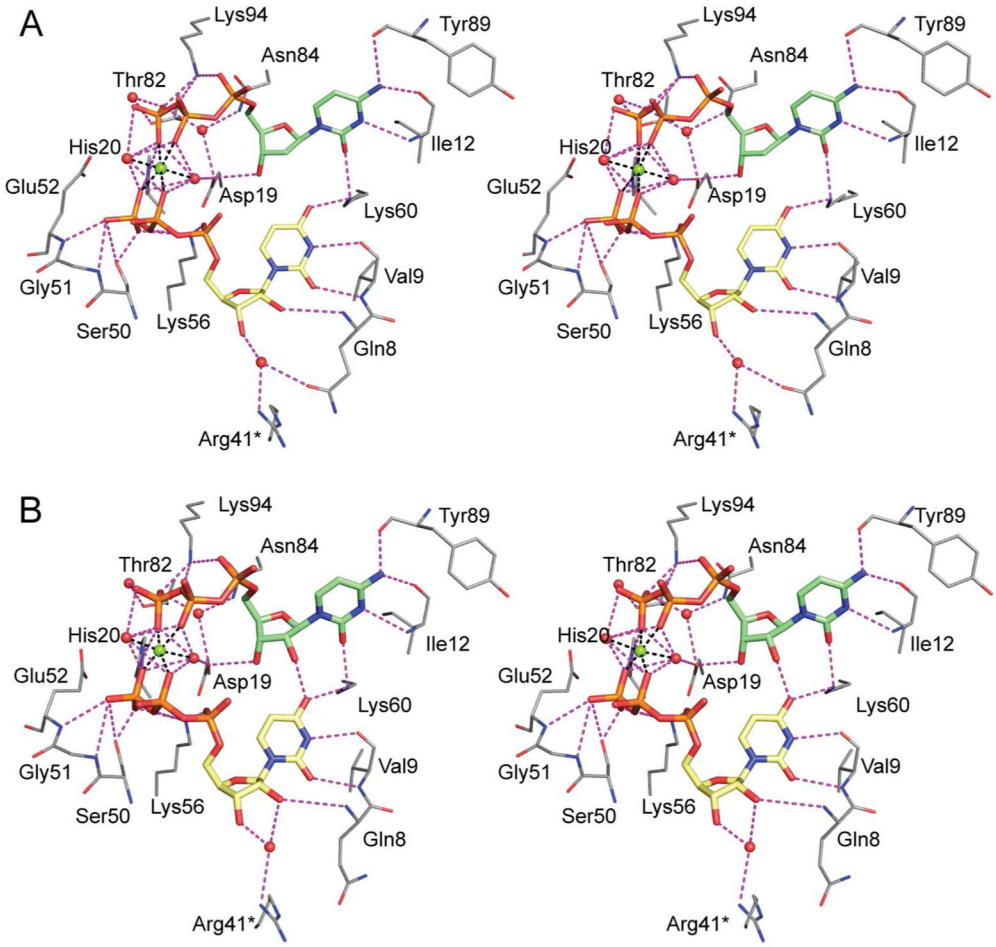

Figure 6.

Stereo view of the nucleotide binding sites in the (A) ATCase•dCTP•UTP•Mg^{2+} and (B) ATCase•CTP•UTP•Mg^{2+} complexes. Polar interactions are shown as magenta dashed lines, the Mg^{2+} as a green sphere, and ordered water as red spheres. The asterisk after Arg41 indicates that this residue is donated from the adjacent regulatory chain in the dimer.

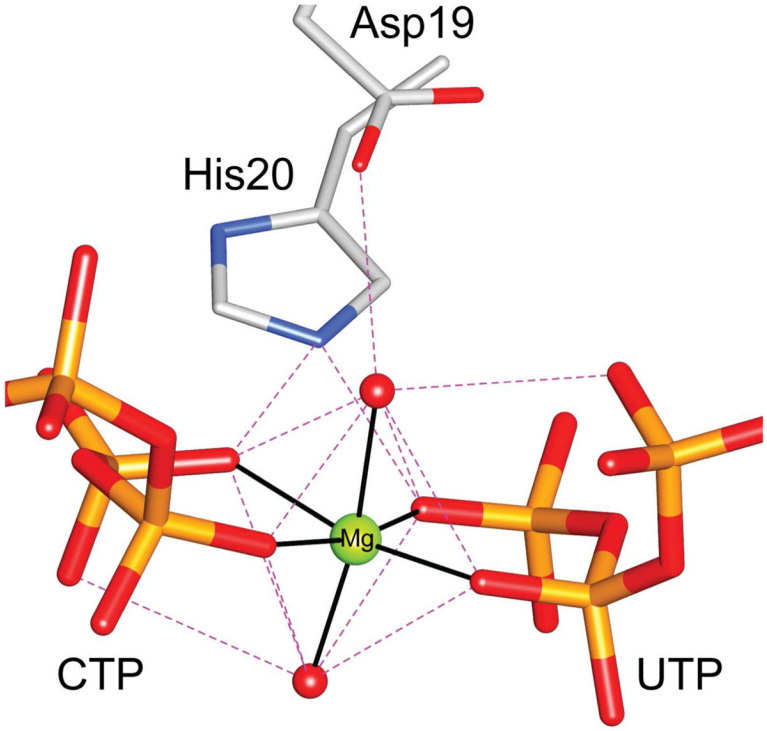

Figure 7.
The metal binding site in the allosteric regulatory site of ATCase. For clarity only the triphosphate portion of the nucleotides are shown.

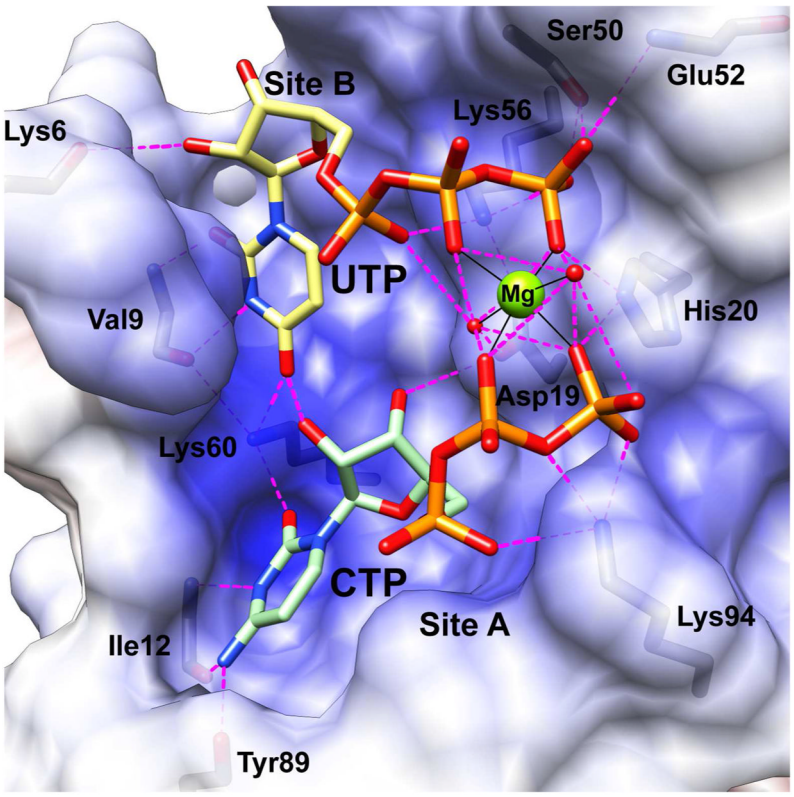

Figure 8.

X-ray structure of the ATCase•CTP•UTP•Mg^{2+} complex showing the r6 regulatory chain electrostatic potential mapped onto the solvent accessible surface in the absence of ligands, as calculated by Delphi.[30] Also shown are the regulatory site ligands, CTP, UTP, Mg^{2+} and the two water molecules that complete the coordination sphere of the Mg^{2+}. The electrostatic potential of the structure was mapped onto the surface (−10 kT/e (red) to +10 kT/e (blue)).

Table 1

Data collection and refinement statistics[a]

	ATCase•dCTP	ATCase•CTP	ATCase•dCTP•UTP•Mg^{2+}	ATCase•CTP•UTP•Mg^{2+}
		Data collection statistics		
PDB entry	4FYV	4FYW	4FYX	4FYY
Space group	P321	P321	P321	P321
Wavelength	1.075	1.542	1.075	1.075
Cell Dimensions				
a, b, c (Å)	120.7,120.7,142.5	121.3, 121.3, 142.3	121.2, 121.2, 141.8	121.1, 121.1, 141.4
α, β, γ (°)	90, 90, 120	90, 90, 120	90, 90, 120	90, 90, 120
Resolution (Å)	50 − 2.1 (2.2–2.1)	43.2 − 2.1 (2.2 – 2.1)	50 − 2.1 (2.2 – 2.1)	50 − 1.9 (2.0 – 1.9)
R_{sym}	0.107 (0.562)	0.063 (0.450)	0.145 (0.684)	0.137 (0.608)
Average (I/σ)	15.0 (4.3)	11.8 (2.9)	13.2 (4.1)	11.9 (4.0)
Completeness (%)	99.8 (98.4)	99.7 (100.0)	100.0 (99.6)	100.0 (99.9)
Redundancy	23.1 (21.1)	5.4 (5.3)	22.3 (20.3)	22.0 (19.5)
		Refinement statistics		
Resolution (Å)	49.1 − 2.1	43.2 − 2.1	49.2 − 2.1	49.2 − 1.9
Reflections	70,567	70,733	71,745	89,120
R_{work}/R_{free}	0.176/0.216	0.184/0.229	0.165/0.213	0.193/0.237
Number of atoms				
Protein	7082	7,083	7,149	7,140
Waters	496	571	634	574
R.m.s. deviations				
Bond lengths (Å)	0.009	0.008	0.009	0.007
Angles (°)	1.18	1.13	1.07	1.14
Mean B value ($Å^2$)	54.8	30.0	39.3	41.2
Ligand B value ($Å^2$)[b]				
CTP (r1/r6)	103.5/84.0	44.8/55.5	46.2/40.7	46.3/45.7
UTP (r1/r6)	-	-	46.6/42.0	43.9/47.2
Mg^{2+} (r1/r6)	-	-	47.1/43.4	45.5/44.4

[a] Values in parentheses are for the highest resolution shell.

[b] Occupancies of all ligands were 1.0.